Molecular engineering to improve the charge carrier balance in single-layer silole-based OLEDs†

Laurent Aubouy,[a] Nolwenn Huby,[b] Lionel Hirsch,*[b] Arie van der Lee[c] and Philippe Gerbier*[a]

Received (in Montpellier, France) 15th January 2009, Accepted 31st March 2009
First published as an Advance Article on the web 27th April 2009
DOI: 10.1039/b900780f

We report a molecular engineering study on optical, structural and electrical properties of seven silole derivates aimed at enhancing the charge carrier balance in single-layer devices. By functionalizing two hole-transporting groups, dipyridylamine and anthracene, on the silole ring, we have investigated the influence of both substituents on the hole current. We have concluded that in contrast to dipyridylamine groups, anthracene groups decrease the charge carrier balance since the latter groups not only increase the hole current but also electron contribution. Mixing these hole-transporting groups and doubling their number lead to a novel silole becoming a very efficient emissive layer exhibiting threshold voltage below 3 V and luminous efficiency L_e = 0.8 cd A^{-1} at 7 V.

Introduction

Organic light-emitting diodes (OLEDs) using small molecules or polymers have been intensively pursued after the initial work by Tang, Van Slyke and Burroughes and co-workers[1,2] because of their enormous potential in flat, flexible panels for lighting and displays. The search for efficient and stable, new emitting materials with appropriate emission spectra remains one of the most active areas of these studies. Different strategies have been developed to enhance the efficiency of the devices such as assisted singlet–triplet internal conversion and the balance of charge carriers in the emissive zone. Among them, the approach involving the incorporation of heavy metal complexes has attracted great attention since it provides both very high efficiencies and white emission.[3–8] On the other hand, the balance of charge carriers in the emissive zone has attracted much less attention due to the development of multilayer structures as a response to this issue.[9,10] Indeed, in organic semiconductors, one of the two charge carriers presents a higher mobility compared to the other one. This leads to several drawbacks such as, for instance, the location of the recombination zone close to an electrode, leading to a huge quenching of excitons. It is possible to overcome this problem by using PIN OLED structures. This structure basically consists of a p-doped hole transport layer (p-HTL), an intrinsic electron blocking layer (EBL), emission layer (EML), hole blocking layer (HBL) and an n-doped electron transport layer (n-ETL). The p-doping and n-doping result in high conductivity and Fermi level shift. This leads to high current injection from both electrodes into the organic layers.[11] Nevertheless, this approach suffers some drawbacks due to a large number of interfaces and/or the apparition of segregation phase.

The aim of this work was to design a fluorescent molecule able to transport both charge carriers. In this way, we focussed on silole derivatives since they appear to possess all the requirements to achieve single-layer OLEDs. The siloles[12–15] or silacyclopentadienes are a group of five-membered silacycles that possess σ*–π* conjugation arising from the interaction between the σ* orbital of two exocyclic σ bonds on the silicon atom and the π* orbital of the butadiene moiety.[16] As a consequence, the calculated LUMO level of a silole ring is lower than those of other heterocyclopentadienes, such as pyrrole, furan, and thiophene. Moreover, thanks to its non-aromatic character the π-system of the silole ring is more prone to allow electron delocalization when compared with its thiophene cousins.[17,18] From a structural point of view, because of the non-coplanar structure of 2,3,4,5-tetraarylsiloles, the distances between silole cores of any two adjacent molecules, even in the solid state, are far from the normal π–π interaction distance (*ca.* 3–4 Å).[19] This gives rise to a very interesting photophysical property called aggregation-induced photoluminescence (PL) emission (AIE).[20,21] Because of the AIE characteristics, 2,3,4,5-tetraphenylsiloles can show extremely high PL quantum yields (up to 100%), even in a crystalline form.[22,23] Therefore, 2,3,4,5-tetraphenylsiloles are excellent emitters in the fabrication of electroluminescence (EL) devices, an external quantum efficiency (η_{EL}) up to 8%, close to the theoretical limit for a singlet emitter, being realized with such derivatives in the emissive layer.[24,25] Finally, siloles exhibit very high electron mobilities, exceeding those for the

[a] *Université Montpellier 2, Institut Charles Gerhardt de Montpellier—UMR 5253, CC 007, Place Eugène Bataillon, 34095 Montpellier cedex 5, France. E-mail: gerbier@univ-montp2.fr; Fax: +33 (0)4 67 14 38 52*
[b] *Université Bordeaux 1, Laboratoire d'Intégration du Matériau au Système (IMS)—UMR 5218, Ecole Nationale Supèrieure de Chimie et de Physique de Bordeaux, 16, Avenue Pey Berland, 33607 Pessac Cedex, France. E-mail: lionel.hirsch@ims-bordeaux.fr; Fax: +33 (0)5 40 00 66 31*
[c] *Université Montpellier 2, Institut Européen des Membranes—UMR 5635, CC 047, Place Eugène Bataillon, 34095 Montpellier cedex 5, France. E-mail: avderlee@univ-montp2.fr; Fax: +33 (0)4 67 14 38 52*
† CCDC reference number 725599. For crystallographic data in CIF or other electronic format see DOI: 10.1039/b900780f

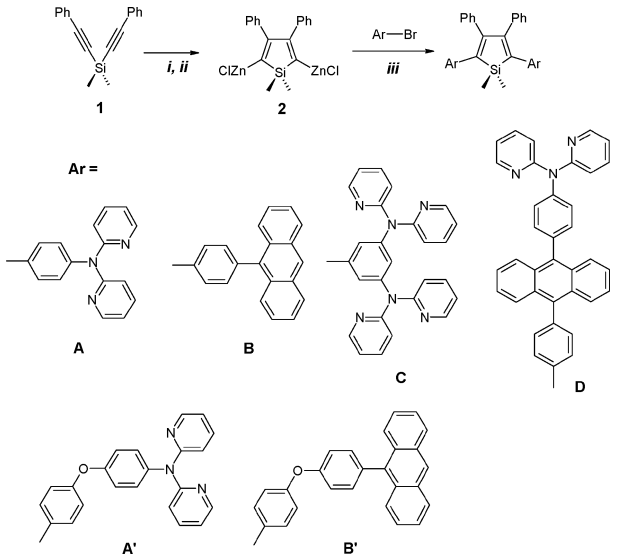

Scheme 1 Tamao's synthetic route to 2,5-difunctionalized siloles: (i) 4 equiv. LiNp, (ii) 4 equiv. $ZnCl_2$·TMEDA, (iii) 2 equiv. ArBr, $PdCl_2(PPh_3)_2$.

well-known tris(8-hydroxyquinoline) aluminium (Alq3), and have been utilized as the electron-transporting layer for EL devices.[26–28]

The results presented in this paper follow previous reports concerning the silole **A** (Scheme 1).[25,27] This molecule is based on a silacyclopentadiene core, which acts both as the emissive and the electron-transporting component, and two dipyridylamino functionalities grafted on each side, which act as hole-transporting groups.[29,30] By associating these two functionalities, we have achieved a sufficient balance of charge to make light from single-layer OLEDs. However, investigations of the temperature dependence and the electron injection barrier dependence have highlighted the weak hole contribution in hole-only devices that is three orders of magnitude lower than the electron one.[27] Since it may be expected that a better balance of charge should improve greatly the efficiency of the devices, we have designed the siloles shown in Schemes 1 and 3 to increase their ambipolar character and, consequently, their hole-transporting properties.[31] Firstly, the dipyridylamino hole-transporting groups were substituted by anthracenyl groups, which can also be considered as good hole-transporters in spite of their displaying an ambipolar character (siloles **B** and **B′**).[32,33] Secondly, we varied the ratio of hole carriers to electron carriers, 1 : 1 for silole **E**, 2 : 1 for siloles **A**, **A′**, **B**, **B′** and 4 : 1 for siloles **C** and **D**. The effect of the conjugation between electron- and hole-transporting moieties was also studied by inserting a disrupting ether bridge between the two (siloles **A** *vs.* **A′** and **B** *vs.* **B′**). Optical and structural properties are systematically correlated to the device performances in order to highlight the influence of the number of hole-transporting groups on the balance of charge carriers.

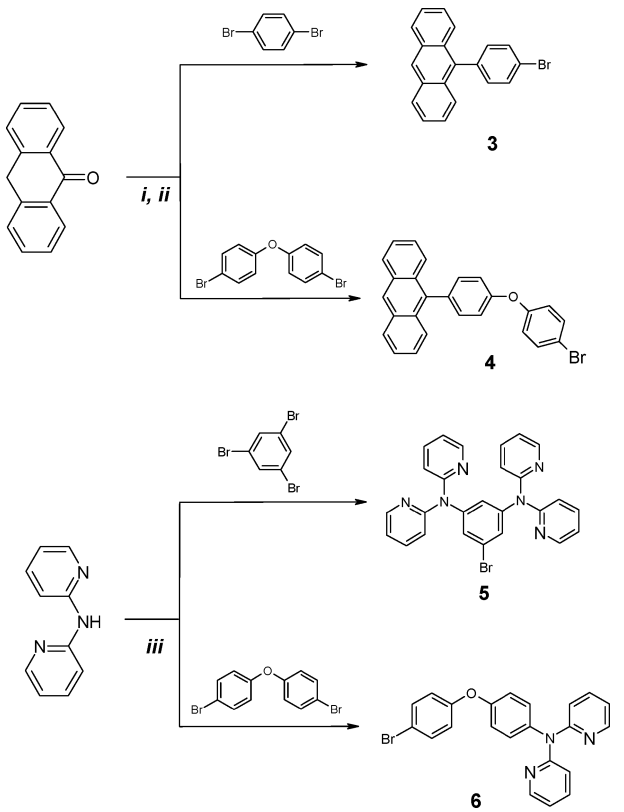

Scheme 2 Syntheses of the hole-transporting functionalities: (i) 1 equiv. n-BuLi, (ii) MeOH, HCl (6 M), (iii) K_2CO_3, $CuSO_4·5H_2O$.

Results and discussion

Syntheses

The siloles **A–D** were conveniently prepared by the method described by Tamao and Yamaguchi and co-workers[34] involving the one-pot reductive intramolecular cyclization of bis(phenylethynyl)silane and the subsequent Pd(0)-catalysed cross-coupling reaction with the desired arylbromide (Scheme 1). The synthesis of 9-(4-bromophenyl)anthracene **3** and 9-[4-(4-bromophenoxy)phenyl]anthracene **4** (Scheme 2) was achieved starting from anthrone by using the procedure described by Murphy *et al.*[35] 3,5-Bis(2,2′-dipyridylamino)bromobenzene **5** and [4-(4-bromo-phenoxy)phenyl]dipyridyn-2-yl-amine **6** (Scheme 2) were synthesized through a modification of the original Ullman reaction.[36,37] The preparation of the asymmetrically 9,10-diarylanthracene **10** (Scheme 3) was achieved

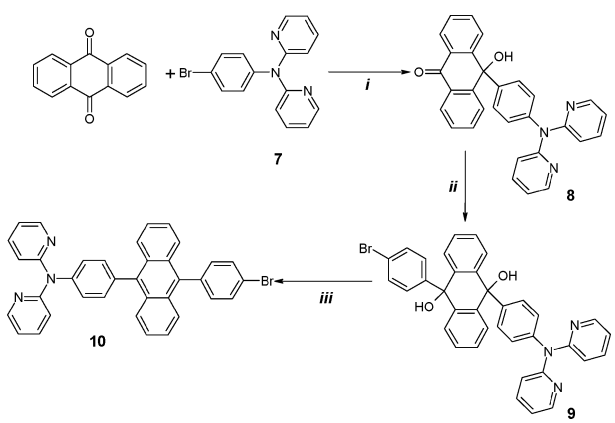

Scheme 3 Synthesis of **10**: (i) *n*-BuLi, (ii) 2 equiv. 1-bromo-4-lithiobenzene, (iii) NaH_2PO_4, KI, glacial acetic acid.

through an adaptation of the procedure described by Smet *et al.*[38,39] It involves firstly the lithiation of compound **7**[25,40] followed by the addition of the resulting lithio derivative to anthraquinone to afford the monoadduct **8** in 43% yield. To this compound, a two-fold excess of 4-bromophenyllithium was added yielding the diol **9**. The excess of 4-bromophenyllithium was necessary to react with the OH group present in the monoadduct **8**. Reduction of the latter using NaH_2PO_2 and KI in refluxing acetic acid afforded **10** as a light yellow solid in 20% yield.

The synthesis of silole **E** (Scheme 4) involves firstly the preparation of the bis-silole derivative **11** by the Tamao–Yamaguchi reaction between the dizincic intermediate **2** and 1.5 equiv. of 1,4-dibromobenzene. The bis(bromophenyl)silole **12** which is formed along with **11** is easily isolated by column chromatography and serves as starting material for other syntheses. The subsequent Suzuki coupling between **11** and the boronic acid derivative **13**[40] afforded the expected bis-silole **E** in good yield.

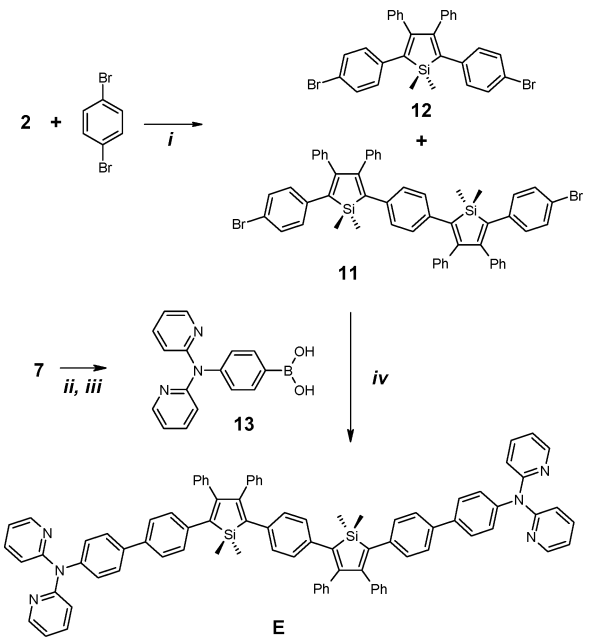

Scheme 4 Synthesis of **E**: (i) $PdCl_2(PPh_3)_2$, (ii) 1 equiv. *n*-BuLi, $B(OMe)_3$, (iii) H_2O, NH_4Cl, (iv) $Pd(PPh_3)_4$, K_2CO_3.

Geometries of siloles

The determination of the conformational preferences of these molecules is of utmost importance for the understanding of their electronic behaviour. Since crystals suitable for a X-ray structure determination could only be obtained for **A**,[41] **B**,[42] and **11**, we turned to density functional theory (DFT) calculations with the B3LYP functional to obtain information about the molecular conformations for the other siloles.[43] Due to the size of the molecules, geometry optimizations without symmetry constrains were performed with the 6-31G basis set to the standard convergence criteria as implemented in Gaussian98.[44] Such calculations were followed by single point runs using a 6-31+G* basis to obtain accurate energies. Structurally characterized siloles, dipyridylamines, and diphenylethers served as benchmarks to test how well the experimentally determined geometry is reproduced by the calculations, and some relevant torsion angles are collected in Table 1.[19] As exemplified with **A** (Fig. 1), all compounds have a propeller-like arrangement of the four phenyl rings, as found in the crystal structures, while the two methyl substituents on the silicon atom are nearly perpendicular to the mean plane of the SiC_4 ring. The torsion angles of the substituted phenyl rings at the 2- and 5-positions of the central silole ring (φ_1) are in

Table 1 Torsion angles [°] in siloles[a]

	A[b]	B[b]	C	D[bd]	E
φ_1[c]	43.4 (44.7)	49.1 (58.4)	38.6	47.8	43.5 (45.1)
φ_2[c]	45.4 (34.3)	—	46.8	50.8 (50.4)	55.5
φ_3[c]	—	77.0 (68.5)	—	71.6 (74.2)	—

[a] Average values. [b] Values from crystal structures (see text) are in parentheses. [c] See Scheme 5. [d] See ref. 45.

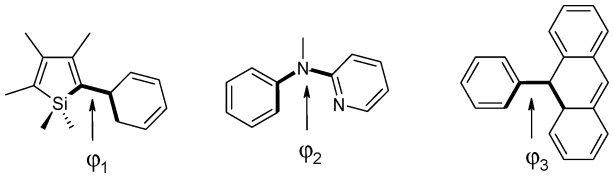

Scheme 5 Location of the torsion angles reported in Table 1.

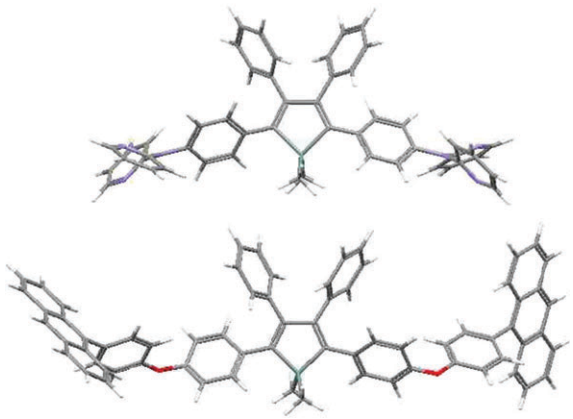

Fig. 1 DFT-optimized (B3LYP-6/31G) molecular structures of siloles **A** (top) and **B′** (bottom).

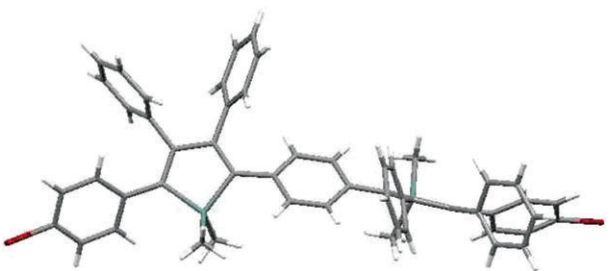

Fig. 2 X-Ray structure of silole **11**. The CH_2Cl_2 crystallization molecule has been removed for the sake of clarity.

Table 2 Main values of the optical properties (UV-visible and fluorescence spectra) in solution and in thin films[a]

Silole	Absorption[b] λ_{max}/nm	PL[b] λ_{max}/nm	Quantum yield[c]	EL λ_{max}/nm	HOMO and (LUMO) levels[d]/eV
A	388 (403)	526 (542)	0.040	545	−5.20 (−2.04)
B	389 (394)	428 (507)	0.015	521	−5.39 (−2.00)
C	379 (385)	503 (511)	0.038	520	−5.32 (−1.79)
D	404 (437)	455 (503)	0.040	518	−5.09 (−1.85)
E	419 (−)	538 (557)	0.002	586	−5.11 (−1.89)
A′	378 (375)	505 (505)	0.006	504	−5.00 (−2.01)
B′	388 (392)	407 (507)	0.020	517	−5.16 (−2.32)

[a] The values recorded with thin solid films are in parentheses. [b] Measured in CH_2Cl_2. [c] Measured in solution, quantum yield relative to perylene (ϕ_{em} = 0.94). [d] From B3LYP-6/31G* DFT calculations.

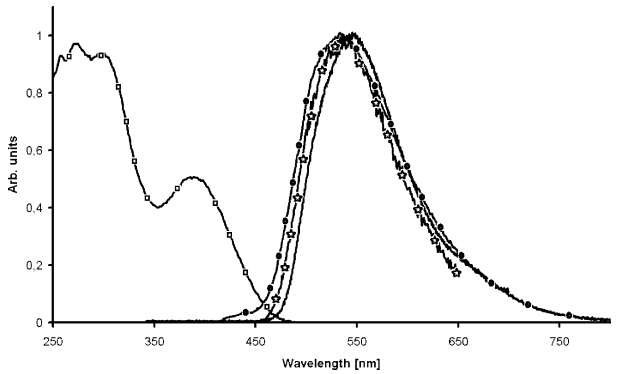

Fig. 3 Normalized UV-visible (□), photoluminescence (in solution ○ and thin film ☆) and electroluminescence (—) spectra of silole A.

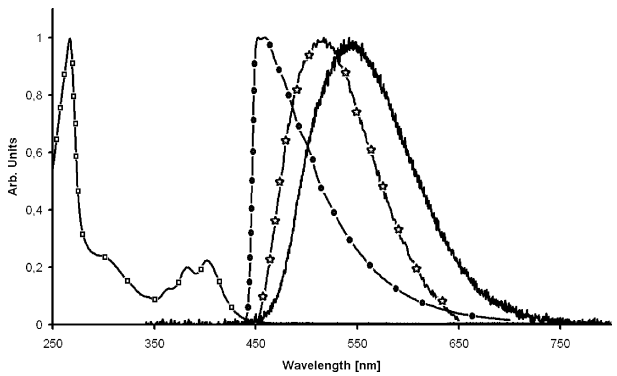

Fig. 4 Normalized UV-visible (□), photoluminescence (in solution: ○ and thin film: ☆) and electroluminescence (—) spectra of silole D.

the range of what is usually observed with tetraarylsiloles (*ca.* 30–60°).

The torsion angles between the anthracene main plane and the adjacent phenyl ring (φ_3) fall well in the range of what is usually observed with related molecules (*ca.* 70°). This is expected to induce a strong reduction of the conjugation between the electron-transporting silole ring and the lateral hole-transporting groups. The same is expected when an ether bridge is inserted between the two electroactive components since the plain planes of the phenyl ring on both sides of the oxygen atom are nearly perpendicular (see Fig. 1). Though no crystal suitable for X-ray diffraction was obtained for the bis-silole **E**, we were able to solve the structure of its precursor **11**. This compound crystallizes along with one CH_2Cl_2 molecule in the *C*2/*c* space group. As seen in Fig. 2, the molecule lies about a two-fold axis that passes through the middle of the central phenyl ring. The torsion angles φ_1 between this ring and the two adjacent siloles have a value of 45.14°. As a result, the two silole rings are nearly perpendicular, which contrasts very strongly with the thiophene analogues that are nearly planar. This situation is also encountered in the optimized geometry of silole **E**.

Optical and electronic properties

The UV-visible absorption, and photoluminescence (PL) spectra have been measured both in solution and thin films. Electroluminescence (EL) spectra were obtained from single layer devices with the structure: ITO/PEDOT:PSS/silole (50 nm)/Ca. The most relevant data obtained from these spectra are collected in Table 2. Fig. 3 and 4 are representative of the two behaviours that are encountered in this series of molecules. As it is seen in Fig. 3, compounds **A**, **A′**, **C** and **E** display a broad absorption band in the range of 368 nm to 389 nm which is characteristic of the $\pi \rightarrow \pi^*$ transition in the silole ring.[34] However, as seen in Fig. 4, in the compounds **B**, **B′** and **D**, this transition is overlapped by the readily recognizable pattern of phenylanthracenes. The comparison of Fig. 3 and 4 reveals that the siloles without anthracene side-groups behave differently from those bearing them. In the first family (siloles **A**, **A′**, **C** and **E**) all the emission spectra are nearly superimposable whatever the excitation mode or the physical state (solution *vs.* thin film). The most important deviation is found with silole **C** in which a shift of *ca.* 9 nm is found between the PL and the EL spectra (Table 2). In the second family (siloles **B**, **B′** and **D**), the PL and EL spectra show differences both in the position of their emission maxima and in their shape, as exemplified in Fig. 4 with silole **D**. In solution, the anthracene moieties appear to be mainly responsible of the emission, as attested by the vibronic coupling seen on the curves. Moreover, it is worth noting that the Stokes shift that is observed with this second family (*ca.* 20–50 nm) is substantially smaller than with the first one (*ca.* 120–140 nm). As usually observed for 2,3,4,5-tetraphenylsiloles, the quantum yields in solution are rather low (Table 2), the lowest value being found with **E** in which two silole rings are present in the structure. This behaviour likely must originate from a resonant photon absorption, since there is a substantial overlap between the absorption and the emission spectra. Moreover this observation, which indicates that the two siloles rings behave independently, is in good agreement with their perpendicular arrangement in the molecular structure (see above).

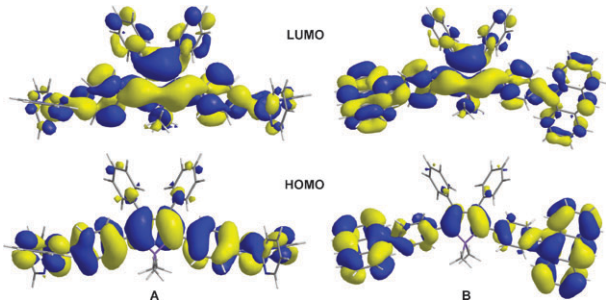

Fig. 5 B3LYP/6-31G*-calculated highest occupied (HOMO) and lowest unoccupied (LUMO) molecular orbitals for siloles **A** and **B**.

Interestingly, the presence of either 9-phenylanthracene or 9,10-diphenylanthracene highly fluorescent subunits (see below) in the molecular structures of siloles **B**, **B′** and **D** has no positive effect on their quantum yields. Along with what is observed in the fluorescence spectra, this indicates that a large amount of energy is transferred from the anthracene chromophores to the silole and then released *via* non-radiative processes. Finally, semi-quantitative measurements of the fluorescence quantum yields on thin films have also been performed. The following sequence was found: **B** ≈ **B′** > **D** > **A** > **A′** > **C** > **DPA** > perylene ≈ **E** where **DPA** (9,10-diphenylanthracene, ϕ_{em} (solution) = 1.00) and **P** perylene (ϕ_{em} (solution) = 0.94)[46] are given for comparison. On account of the AIE phenomenon,[20,21] the siloles display a very strong fluorescence in the solid state that exceeds both DPA and perylene which possess nearly quantitative quantum yields in solution.

To better understand the optical data, we now turn to a description of the main characteristics of the HOMO and LUMO levels as calculated at the DFT level. The analysis of the HOMO and LUMO wavefunctions shown for siloles **A** and **B** in Fig. 5 shows the typical pattern of tetraphenylsiloles.[47,48] The HOMO wavefunctions show a very similar spatial distribution with an antibonding character between the silole ring and the phenyl rings located at the 2,5-positions. The same similarity is found with the LUMO wavefunctions in which bonding character is observed between the silole ring and the adjacent phenyl rings. The energies of the HOMO and LUMO orbitals (Table 2), which do not vary to any great extent upon modification of the substituents, are in the range of what is usually reported for tetraarylsiloles. The

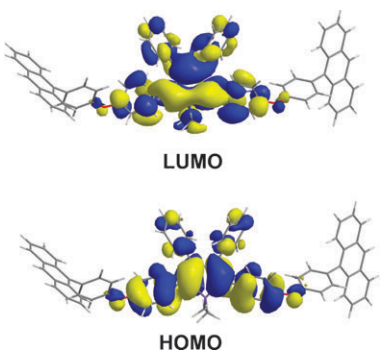

Fig. 6 B3LYP/6-31G*-calculated HOMO and LUMO molecular orbitals for silole **B′**.

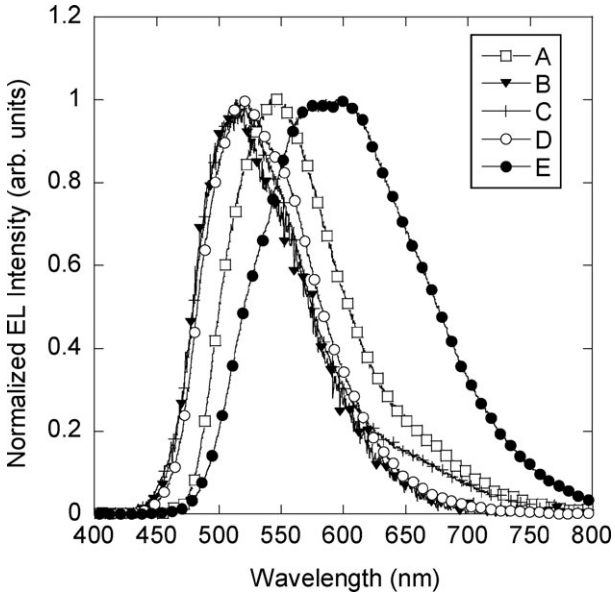

Fig. 7 EL spectra from devices ITO/PEDOT:PSS/silole (50 nm)/Ca.

examination of the wavefunctions calculated for siloles **A′** and **B′** (Fig. 6 for **B′**) shows a nearly identical orbital distribution on the tetraphenylsilole core. However, in contrast to their parents **A** and **B**, very little electron probability density is found on either the dipyridylamino or the phenylanthracene moieties. This illustrates the expected disruption of the conjugation brought about by the diphenylether bridges, and the reason why the emission maximum of these two molecules is blue-shifted by 20 nm compared to their parents **A** and **B**.

Electroluminescence properties and balance of charge carriers

In order to study the EL properties, single layer devices were investigated, with the following structure: ITO/PEDOT:PSS/silole (50 nm)/Ca. The electroluminescent spectra are shown in Fig. 7. As observed during the photoluminescence studies, only the silole ring contributes to the emission and the device based on molecule **A** is 20 nm red-shifted compared to the others. All the emissions correspond to the yellow–green domain in the chromatic diagram of the *Commission Internationale de l'Eclairage*. Their corresponding current density–voltage and luminance–voltage are presented in Fig. 8(a) and 8(b), respectively. When compared with the calculated HOMO and LUMO energy levels of the siloles (see Table 2), the high work function of the anode ITO/PEDOT:PSS (−5.2 eV) and the low work function of the calcium cathode (−2.9 eV) should favour the injection of both charge carriers in the active layer. As a consequence, threshold voltage values generally below 4V are necessary for the detection of luminance of the device (Table 3). Moreover, with the exception of siloles **C** and **E**, all the molecules presented here display quite good luminous efficiencies (L_e) for single-layer devices. In terms of performances, **D** exhibits the best values with a threshold voltage below 3 V and a luminous efficiency L_e of 0.75 cd A^{-1} at 7 V. In contrast, **C** and **E** are weakly electroluminescent. Indeed, these molecules need higher applied voltages to reach the same order of current density than with **A**, **B** or **D**.

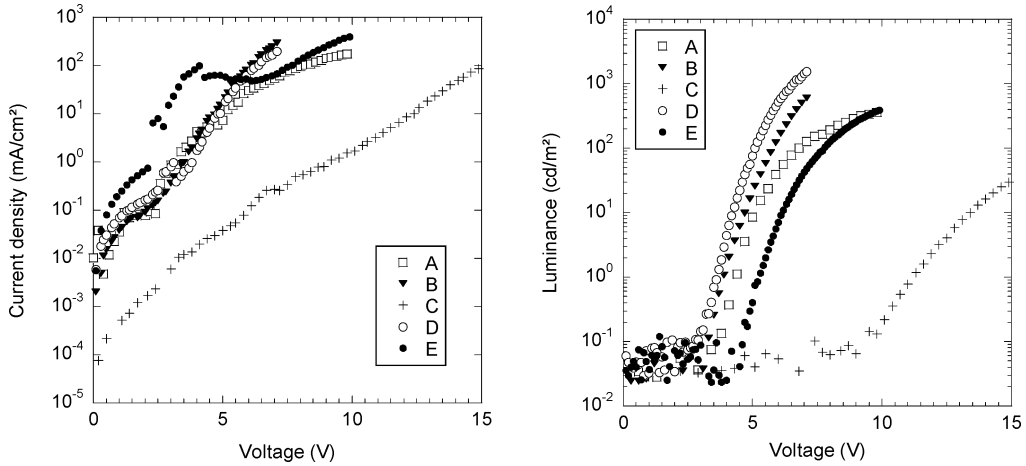

Fig. 8 (a) Current density–voltage characteristics for devices based on /PEDOT:PSS/silole (50 nm)/Ca, and (b) corresponding luminance–voltage characteristics.

Table 3 The luminance (L), luminous efficiency (L_e) and energetic efficiency (R_e) of siloles operating in ITO/PEDOT:PSS/silole/Ca OLEDs[a]

Silole	V_{th}/V	L/cd m^{-2}	L_e/cd A^{-1}	R_e/lm W^{-1}
A	3.5	26 (370)[b]	0.17 (0.20)[b]	0.095 (0.06)[b]
B	3.1	25 (350)[b]	0.16 (0.18)[b]	0.100 (0.09)[b]
C	9	8 (74)[c]	0.05 (0.036)[c]	0.012 (0.015)[c]
D	2.9	80 (1550)[c]	0.52 (0.75)[c]	0.320 (0.35)[c]
E	4.5	−(86)[c]	−(0.09)[c]	—
A′	18	5 (5)[b]	0.03 (0.03)[b]	0.003 (0.003)[b]
B′	4.2	21 (290)[c]	0.14 (0;19)[c]	0.060 (0.060)[c]

[a] Values measured at a current density of 20 mA cm^{-2}. [b] Value in parentheses measured at 100 mA cm^{-2}. [c] Value in parentheses measured at 200 mA cm^{-2}.

To better understand the origin of this different behaviour and to try to outline the relationships that may exist between the molecular structure and the balance of charge carriers in this series of molecules, one has to consider the factors that determine the efficiency of an OLED. Actually, this may approximately be calculated by the following equation:[49,50]

$$\eta_{external} = \gamma \times \eta_{recomb} \times \eta_{ST} \times \eta_{optical} \times \Phi_{PL} \quad (1)$$

where $\eta_{external}$ is the total power efficiency of the device, γ is the balance of charge carrier, η_{recomb} represents the recombination probability of injected holes and electrons, η_{ST} is the ratio of singlet and triplet excitons contributing to the radiative recombination, $\eta_{optical}$ is the efficiency of the optical out-coupling from the device, and Φ_{PL} is the quantum yield of fluorescence of the emissive material. By spin statistics, η_{ST}, which is the ratio of singlet to triplet excitons, should be $\eta_{ST} = 0.25$, since parallel spin pairs will recombine to triplet excitons while antiparallel spin pairs will recombine to singlet and triplet excitons. Thus, for fluorescent emitters, we find $\eta_{ST} = 0.25$, which is a severe limitation of quantum efficiency of an OLED. Concerning the optical outcoupling efficiency, a simple estimation regarding the OLED as a classical optics device shows that a flat device with typical refractive index of the organic layers of 1.7, deposited on ITO/glass, achieves approximately 20% outcoupling. Therefore, the first factor that defines the efficiency of an OLED on which we can play from a molecular engineering point of view is the balance of the charge carrier (γ).

To analyse the result of molecular engineering on the silole core in terms of the balance of charge carriers, one has still to take into account both the charge transport processes and the quantum yield of fluorescence in the solid state of each molecule. Concerning the first issue, at least two parameters have to be taken into consideration: the orbital energy levels and the organization of the molecules in the thin film.[27,42,51,52] In previous work we have studied the transport properties of siloles **A** and **B**.[42] Actually, they are very close in behaviour on account of their similarities, both in terms of molecular organization (they form amorphous films) and in terms of the energy levels and orbital distribution (see above).[27,42,51] Therefore, it seems reasonable to set the factor η_{recomb} in eqn (1) to the same arbitrary value for all the series of molecules studied here. In this way, the comparison of the luminous efficiencies corrected by the relative solid-state Φ_{PL} value should allow an estimation of the effect of molecular engineering on the balance of charge carriers.

From semi-quantitative measurements we have found the following sequence for the solid-state photoluminescence quantum yield Φ_{PL}: **B** ≈ **B′** > **D** > **A** > **A′** > **C** > **E**. By using the procedure of normalization described in the

Table 4 The luminous efficiency (L_e), relative solid-state PL quantum yield (Φ_{PL}) and the hole carrier to the electron carrier formal ratio (h^+ to e^-) of siloles operating in ITO/PEDOT:PSS/silole/Ca OLEDs

Silole	L_e[a]/cd A^{-1}	Relative solid-state Φ_{PL}	L_e/Φ_{PL}/cd A^{-1}	$h^+ : e^{-b}$
A	0.17	0.44	0.39	2
B	0.16	1.00	0.16	2
C	0.05	<0.05	>1.00	4
D	0.52	0.67	0.78	4
E	—	—	—	1
A′	0.03	0.36	0.08	2
B′	0.14	1.00	0.14	2

[a] Values measured at a current density of 20 mA cm^{-2}. [b] A silole ring accounts for 1 e^- whereas either an anthracenyl or a dipyridylamino side-group accounts for 1 h^+.

experimental section, we have found that the photoluminescence intensity of **B** is *ca.* 1.5 times higher than that of **D**, *ca.* 2.3 times higher than that of **A**, *ca.* 2.8 times higher than that of **A′** and more than 20 times higher than that of **C** (the value for **E** is not given since it is of the same order as the error for the measurement). Therefore, the ratio L_e over Φ_{PL} should give a good indication as to the correlation between the balance of charge carriers in the device and the hole carrier moieties (h^+: dipyridylamino or anthracenyl side-groups) over the electron carrier moieties (e^-: silole ring) present in the molecular structure (Table 4).

From an examination of Table 4, it appears that the major trend is that the higher the h^+ to e^- ratio, the more the balance of charges appears to be improved. This result is in good agreement with the fact that the silole ring possesses an exceptional electron carrier ability[26–28] greatly exceeding the hole carrier ability of the organic groups grafted to it. As a consequence a large number of hole-transporting groups are needed to correct the balance of charge. Therefore, the silole **D** in which the h^+ to e^- ratio is equal to 4 displays the best luminous efficiency. This is not so surprising since silole **D** may also be considered as silole **B** bearing two additional hole-transporting side-groups. In the case of the silole **C**, in spite of a similar ratio, the performances are disappointing since luminance and efficiencies (see Table 2) are one order of magnitude lower than **A** and **B** at 20 mA cm^{-2}. Moreover the current density is considerably lower than that observed with the other molecules at a given applied voltage. This phenomenon may be attributed to two main reasons: (i) this silole possesses a weak solid-state Φ_{PL} when compared to **D**, and (ii) the four dypirydilamino groups generate strong steric hindrance which disfavours the electron transfer between the silole rings in the device.

The comparison of siloles **A** and **B** in which the h^+ to e^- ratio is equal to 2 allows us to estimate the relative ability of the side-group to transport holes. They are both equivalently efficient in OLEDs but **A** is characterized by an L_e to Φ_{PL} ratio of 0.39 whereas that for **B** is 0.16. In other words, the dipyridylamino groups appear to be more efficient than anthracenyl groups as hole carriers in correcting the balance of charges in silole-based devices. This may originate from the fact that anthracene entities not only enhance the hole current compared to the dipyridylamine ones, but also increase the electron current, leading to the smallest correction of the balance of charge carriers. The comparison of siloles **A**, **A′**, **B** and **B′** allows us now to evaluate the importance of the conjugation between both charge carriers since the presence of the diphenyl bridge has been shown to isolate both moieties from an electronic point of view (see above). The disruption of the conjugation in silole **A′** is accompanied by a marked decrease in efficiency when compared to **A**, while the solid-state Φ_{PL} of both are close enough. In contrast to that, the same modification only weakly affects the efficiency of the devices based on siloles **B** and **B′**.

Conclusions

With the goal to improve the balance of charge carrier in single layer silole-based OLEDs, we have synthesized a series of ambipolar molecules, in which the silole central core acts as an electron-transporting unit, whereas either dipyridylamino or anthracene groups act as hole-transporting groups. The siloles were conveniently prepared by the method described by Tamao and Yamaguchi. The studies have clearly outlined some trends.

The presence of either dipyridylamino or anthracene groups in the molecular structure of the siloles brings about a significant improvement of the balance of charge in the devices.

The dipyridylamino groups appear to be more efficient than the anthracenyl groups since they are capable of ambipolar transport.

The ratio of hole-transporting groups to siloles effectively improves the balance of charge, but the overall effect is not easy to forecast since intermolecular parameters are also involved in charge transport.

The conjugation between electron- and hole-transporting groups appears to be important for achieving high efficiency. This indicates that there is synergy between the various components of the molecule.

As a consequence, we have synthesized the silole **D**, in which two anthracene groups and two dipyridylamino groups are connected to the central silole core through a conjugated backbone. This silole, operating in a single-layer OLED, exhibited an excellent performance with a threshold voltage below 3 V and luminous efficiency L_e = 0.8 cd A^{-1} at 7 V. Additional studies are in progress to better understand the interplay between the charge-transporting groups in these ambipolar molecules.

Experimental

General methods and device performance measurements

Solvents were distilled prior to use. THF and ether were dried over sodium–benzophenone, and distilled under argon. All reactions were carried out under an argon atmosphere. ^1H, ^{13}C and ^{29}Si NMR spectra were recorded on a Bruker Advance 200 DPX spectrometer, the FT-IR spectra on a Thermo Nicolet Avatar 320 spectrometer, the UV-visible spectra on a Secomam Anthelie instrument and the MS spectra on a Jeol JMS-DX 300 spectrometer. Fluorescence spectra in thin films were recorded with an Edinburgh Instruments Ltd spectrofluorimeter. Absorption spectra in thin film were realized with an UV-visible SAFAS Monaco 190 DES spectrometer. Current–voltage (*I–V*) characteristics were recorded using a Keithley 4200 Semiconductor analyser, and luminance–voltage (*L–V*) with a photodiode calibrated with a Minolta CS-100 luminancemeter. Electroluminescence (EL) spectra were measured using an Ocean Optics HR2000 CCD spectrometer. All electroluminescent devices were fabricated and characterized in a glove box under nitrogen with [O_2] and [H_2O] less than 0.1 ppm.

The semi-quantitative solid-state quantum yields have been measured on evaporated films of the same thickness and corrected by the corresponding absorption coefficient at the excitation wavelength (380 nm). In order to compare materials, care was taken concerning the experimental conditions.

Spectrofluorimeter parameters were kept unchanged from one sample to another, thickness of the thin films were the same and the fluorescence spectrum of each molecule was corrected by the corresponding absorption coefficient at the excitation wavelength. An excitation wavelength at 380 nm was selected, since all maxima absorption bands are localized in this domain.

Syntheses

9-[4-(4-Bromophenoxy)phenyl]anthracene (4). A solution of *n*-BuLi (2.5 M) in hexane (7.7 mL, 19 mmol) was added to an ethereal solution (70 mL) of 4,4′-dibromodiphenylether (6.25 g, 19 mmol) at −78 °C. The reaction mixture was stirred for 0.5 h at this temperature and anthrone was added in small portions (3 g, 15 mmol). This mixture was left under stirring for 3 h at −78 °C and the temperature was allowed to slowly reach room temperature. An aqueous solution of HCl (0.5 M) was then added to the reaction mixture until a pH of 4–5 was reached and extracted with Et_2O. After the usual processing, the resulting residue was subjected to silica gel column chromatography (CH_2Cl_2–pentane 10 : 90) to give **4** as a white–yellow solid (yield: 50%). Mp: 149 °C. ^{1}H NMR ($CDCl_3$, δ, ppm): 8.54 (s, 1H), 8.09 (d, ^3J(H,H) = 8, 2H), 7.75 (d, ^3J(H,H) = 8 Hz, 1H), 7.60–7.37 (m, 8H), 7.23 (d, ^3J(H,H) = 9 Hz, 2H), 7.12 (d, ^3J(H,H) = 9 Hz, 2H).^{13}C NMR ($CDCl_3$, δ, ppm): 158.81, 156.71, 136.56, 134.35, 133.27, 133.15, 131.79, 130.79, 128.83, 127.13, 127.07, 125.86, 125.55, 121.33, 119.01, 116.45. HRMS (FAB+, *m*-nitrobenzyl alcohol matrix) *m*/*z*: calcd for $[M + H]^+$ $C_{26}H_{17}BrO$: 424.0463; found: 424.0456.

[4-(4-Bromophenoxy)phenyl]dipyridyn-2-yl-amine (6). A mixture of 4,4′-dibromodiphenylether (7.14 g, 21.7 mmol), di-2-pyridylamine (1.50 g, 8.70 mmol), K_2CO_3 (1.40 g, 10.4 mmol) and $CuSO_4{\cdot}5H_2O$ (0.217 g, 0.87 mmol) in water (20 mL) and CH_2Cl_2 (100 mL) was stirred well and evaporated to dryness under vacuum. The mixture was ground in a mortar and 3–5 drops of CH_2Cl_2 were added to this mixture. The mixture was heated in a Schlenk tube at 210 °C for 6 h. After being cooled at room temperature, the mixture was dissolved in CH_2Cl_2 (100 mL) and water (100 mL) and extracted. After evaporation of the solvent, the residue was subjected to column chromatography CH_2Cl_2–THF (95 : 5) to afford compound **6** as a white solid (yield: 80%). Mp: 102 °C. ^{1}H NMR ($CDCl_3$, δ, ppm): 8.33 (dd, ^3J(H,H) = 6, ^3J(H,H) = 2 Hz, 2H), 7.62 (td, ^3J(H,H) = 7, ^3J(H,H) = 2 Hz, 2H), 7.47 (d, ^3J(H,H) = 9 Hz, 2H), 7.21 (d, ^3J(H,H) = 6 Hz, 2H), 7.00–6.81 (m, 8H).^{13}C NMR ($CDCl_3$, δ, ppm): 157.99, 156.17, 154.50, 148.50, 148.47, 140.33, 137.63, 128.92, 120.82, 119.84, 118.15, 116.71, 115.95. HRMS (FAB+, *m*-nitrobenzyl alcohol matrix) *m*/*z*: calcd for $[M + H]^+$ $C_{22}H_{16}BrN_3O$: 418.0550; found: 418.0547.

[4-(Dipyridin-2-yl-amino)phenyl]-10-hydroxyanthracen-9-one (8). A solution of *n*-BuLi (2.5 M) in hexane (10.5 mL, 26 mmol) was added to a THF solution (100 mL) of 4-(2,2′-dipyridylamino)bromobenzene **7**[25,40] (7 g, 21 mmol) at −78 °C. The reaction mixture was stirred for 1 h at this temperature. A THF solution (150 mL) of anthraquinone (8.73 g, 42 mmol) was then added to this mixture and left under stirring for 8 h while allowing the temperature to slowly reach room temperature. An aqueous solution of HCl (1 M) was then added to the reaction mixture until a pH of 4–5 was reached and extracted with Et_2O. After the usual processing, the resulting residue was subjected to a silica gel column chromatography (CH_2Cl_2–THF gradient 97 : 3 to 90 : 10) to give **8** as a light yellow powder (yield: 43%). Mp: 265–267 °C. ^{1}H NMR ($CDCl_3$, δ, ppm): 8.35–8.09 (m, 4H), 7.77 (dd, ^3J(H,H) = 8, ^3J(H,H) = 1 Hz, 2H), 7.62 (td, ^3J(H,H) = 7, ^3J(H,H) = 2 Hz, 2H), 7.58–7.48 (m, 4H), 7.37 (d, ^3J(H,H) = 9 Hz, 2H), 7.10 (d, ^3J(H,H) = 9 Hz, 2H), 7.00–6.89 (m, 4H), 2.93 (s, 1H).^{13}C NMR ($CDCl_3$, δ, ppm): 182.32, 151.40, 148.71, 147.94, 138.45, 134.53, 130.75, 130.36, 128.71, 128.60, 127.37, 127.21, 126.65, 118.83, 117.04, 116.57, 73.5. HRMS (FAB+, *m*-nitrobenzyl alcohol matrix) *m*/*z*: calcd for $[M + H]^+$ $C_{30}H_{22}N_3O_2$: 455.5227; found: 456.1704.

4-[10-(4-Bromophenyl)anthracen-9-yl]phenyldipyridin-2-yl-amine (10). A solution of *n*-BuLi (2.5 M) in hexane (10 mL, 25 mmol) was added to a THF solution (50 mL) of 1,4-dibromobenzene (5.92 g, 25 mmol) at −78 °C. The reaction mixture was stirred for 1 h at this temperature and added *via* a cannula to a THF solution (100 mL) of **8** (3.26 g, 7.1 mmol) also at −78 °C. This mixture was stirred for 8 h while allowing the temperature to slowly reach room temperature, then treated with aqueous HCl (1 M) to pH 4–5 and extracted with ether. The combined organic layers are dried over $MgSO_4$ and evaporated under vacuum to afford compound **9** as a viscous oil. The residue was then dissolved in glacial acetic acid (60 mL), treated with NaH_2PO_4 (8.44 g, 95 mmol) and KI (4.22 g, 25 mmol), and heated to reflux for 20 min. After cooling, the reaction mixture was treated with cold water (300 mL) and extracted with CH_2Cl_2. After the usual processing, the resulting residue was subjected to silica gel column chromatography (CH_2Cl_2–MeOH 99 : 1) to give **10** as a light yellow powder (yield: 20%). Mp: 267 °C. ^{1}H NMR ($CDCl_3$, δ, ppm): 8.42 (dd, ^3J(H,H) = 6, ^3J(H,H) = 2 Hz, 2H), 7.93–7.62 (m, 8H), 7.53–7.39 (m, 10H), 7.21 (d, ^3J(H,H) = 7 Hz, 2H), 7.08 (td, ^3J(H,H) = 7, ^3J(H,H) = 2 Hz, 2H). ^{13}C NMR ($CDCl_3$, δ, ppm): 158.66, 148.85, 144.99, 138.46, 138.05, 136.04, 135.86, 133.49, 132.73, 132.06, 130.31, 130.16, 127.39, 127.07, 126.95, 125.73, 125.59, 122.05, 118.86, 117.81, 116.41. HRMS (FAB+, *m*-nitrobenzyl alcohol matrix) *m*/*z*: calcd for $[M + H]^+$ $C_{36}H_{24}N_3Br$: 577.5097; found: 578.1204.

2-[4-(5-(4-Bromophenyl)-1,1-dimethyl-3,4-diphenyl)silol-2-yl)-phenyl)-5-(4-bromophenyl)]-1,1-dimethyl-3,4-diphenylsilole (11). A mixture of lithium (0.055 g, 8 mmol) and naphthalene (1.03 g, 8 mmol) in THF (15 mL) was stirred at room temperature under argon for 5 h to form a deep green solution of lithium naphthalenide. To this mixture was added bis-(phenylethynyl)dimethylsilane **1** (0.50 g, 2 mmol) in THF (10 mL). After stirring for 10 min, the reaction mixture was cooled to 0 °C and [ZnCl2(tmen)] (tmen = *N*,*N*,*N*′,*N*′-tetramethylenediamine) (2.01 g, 8 mmol) was added, followed by an addition of THF (20 mL). After stirring for an hour at room temperature, a solution of 1,4-dibromobenzene (0.80 g, 34 mmol) in THF (20 mL) and $[PdCl_2(PPh_3)_2]$ (0.10 g, 0.13 mmol) were successively added. The mixture was heated

under reflux and stirred for 20 h. After hydrolysis by water, the mixture was extracted with Et_2O. After evaporation of the solvents, the resulting residue was subjected to silica gel column chromatography (pentane–CH_2Cl_2 95 : 5) to yield **11** and the silole **12** as separate solids. The siloles were each recrystallized from a hexane–CH_2Cl_2 mixture to give **11** as dark yellow crystals (yield: 30%) and **12** as light yellow crystals (yield: 20%). Characterization of silole **11**: Mp: 310 °C. UV-visible (λ_{max}, nm, logε): 255 (5.46), 399 (5.20). ^{1}H NMR ($CDCl_3$, δ, ppm): 7.15 (d, ^3J(H,H) = 9 Hz, 4H), 6.96–6.86 (m, 12H), 6.74–6.64 (m, 12H), 6.58 (s, 4H), 0.35 (s, 1H).^{13}C NMR ($CDCl_3$, δ, ppm): 155.14, 153.86, 142.14, 140.60, 139.26, 139.15, 138.84, 137.38, 131.46, 130.82, 130.32, 130.25, 128.93, 127.92, 127.82, 126.77, 126.63, 119.72, −3.31. ^{29}Si NMR ($CDCl_3$, δ, ppm): 8.09. HRMS (FAB+, *m*-nitrobenzyl alcohol matrix) *m*/*z*: calcd for $[M + H]^+$ $C_{54}H_{44}Br_2Si_2$: 906.1348; found: 906.1330. Characterization of silole **11**: the synthesis of this compound was previously described starting from 1-bromo-4-iodobenzene.[53] Mp: 224 °C. UV-visible (λ_{max}, nm, logε): 250 (5.54), 361 (5.23). ^{1}H NMR ($CDCl_3$, δ, ppm): 7.28 (d, ^3J(H,H) = 9 Hz, 4H), 7.10–7.02 (m, 6H), 6.81–6.75 (m, 8H), 0.47 (s, 1H).^{13}C NMR ($CDCl_3$, δ, ppm): 154.90, 141.17, 139.04, 138.57, 131.56, 130.78, 130.24, 128.02, 126.94, 119.95, −3.52. ^{29}Si NMR ($CDCl_3$, δ, ppm): 8.23. HRMS (FAB+, *m*-nitrobenzyl alcohol matrix) *m*/*z*: calcd for $[M + H]^+$ $C_{30}H_{18}Br_2Si$: 571.9996; found: 571.9985.

Silole A′. Same procedure as for silole **B**, using a solution of *p*-2,2′-dipyridylaminophenyl-4-bromophenylether **6**[51] (1.87 g, 4.4 mmol) in THF (20 mL). After evaporation of the solvents, the resulting residue was firstly subjected to silica gel column chromatography (MeOH–CH_2Cl_2 3 : 97) followed by an alumina column (THF–CH_2Cl_2 5 : 95) to give **A′** as a bright yellow powder (yield: 42%). Mp: 128 °C. UV-visible (λ_{max}, nm, logε): 277 (5.70), 377 (5.20). ^{1}H NMR ($CDCl_3$, δ, ppm): 8.35 (dd, ^3J(H,H) = 6, ^3J(H,H) = 2 Hz, 4H), 7.58 (td, ^3J(H,H) = 7, ^3J(H,H) = 2 Hz, 4H), 7.16 (d, ^3J(H,H) = 9 Hz, 4H), 7.14–6.86 (m, 30H), 0.52 (s, 6H).^{13}C NMR ($CDCl_3$, δ, ppm): 158.13, 155.05, 154.67, 153.77, 148.47, 140.48, 139.84, 138.88, 137.50, 135.11, 132.16, 132.06, 128.86, 127.53, 126.28, 119.69, 118.68, 117.98, 116.66, −3.60. ^{29}Si NMR ($CDCl_3$, δ, ppm): 7.87. MS (FAB+, *m*-nitrobenzyl alcohol matrix) *m*/*z*: 937 $[M + H]^+$. Analysis calcd for $C_{62}H_{48}N_6O_2Si$: 79.46 %C, 5.16 %H, 8.97 %N; found: 79.01 %C, 5.29 %H, 8.82 %N.

Silole B. A mixture of lithium (0.055 g, 8 mmol) and naphthalene (1.03 g, 8 mmol) in THF (15 mL) was stirred at room temperature under argon for 5 h to form a deep green solution of lithium naphthalenide. To this mixture was added bis(phenylethynyl)dimethylsilane **1** (0.50 g, 2 mmol) in THF (10 mL). After stirring for 10 min, the reaction mixture was cooled to 0 °C and [$ZnCl_2$(tmen)] (tmen = *N*,*N*,*N*′,*N*′-tetramethylenediamine) (2.01 g, 8 mmol) was added, followed by an addition of THF (20 mL). After stirring for an hour at room temperature, a solution of 9-(4-bromophenyl)anthracene **3**[35] (1.59 g, 4.8 mmol) in THF (20 mL) and [$PdCl_2(PPh_3)_2$] (0.10 g, 0.13 mmol) were successively added. The mixture was heated under reflux and stirred for 20 h. After hydrolysis by water, the mixture was extracted with Et_2O. After evaporation of the solvents, the resulting residue was subjected to silica gel column chromatography (pentane–CH_2Cl_2 85 : 15) and recrystallized from a hexane–CH_2Cl_2 mixture to give **B** as a yellow crystalline powder (yield: 35%). Mp: 333 °C. UV-visible (λ_{max}, nm, logε): 254 (6.37), 352 (5.22), 368 (5.43), 386 (5.50). ^{1}H NMR ($CDCl_3$, δ, ppm): 8.51 (s, 2H), 8.07 (d, ^3J(H,H) = 8 Hz, 4H), 7.72 (d, ^3J(H,H) = 8 Hz, 4H), 7.53–7.37 (m, 8H), 7.28–7.00 (m, 18H), 0.77 (s, 6H).^{13}C NMR ($CDCl_3$, δ, ppm): 155.02, 146.18, 142.73, 139.58, 139.39, 137.53, 135.22, 133.80, 131.31, 130.62, 130.55, 129.18, 128.72, 127.90, 127.33, 126.81, 125.61, 125.47, −3.07. ^{29}Si ($CDCl_3$, δ, ppm): 2.80. MS (FAB+, *m*-nitrobenzyl alcohol matrix) *m*/*z*: 766 $[M]^+$. Analysis calcd for $C_{58}H_{42}Si$: 90.82 %C, 5.52 %H; found: 90.54 %C, 5.62 %H.

Silole B′. Same procedure as for silole **B**, using a solution of **4** (2.04 g, 4.8 mmol) in THF (20 mL). After evaporation of the solvents, the resulting residue was firstly subjected to silica gel column chromatography (pentane–CH_2Cl_2 80 : 20) and recrystallized from hexane–CH_2Cl_2 to give **B′** as a yellow powder (yield: 89%). Mp: 264 °C. UV-visible (λ_{max}, nm, logε): 257 (6.47), 350 (4.95), 362 (5.13), 385 (5.10). ^{1}H NMR ($CDCl_3$, δ, ppm): 8.54 (s, 2H), 8.09 (d, ^3J(H,H) = 8 Hz, 4H), 7.76 (d, ^3J(H,H) = 8 Hz, 4H), 7.55–7.38 (m, 12H), 7.24 (d, ^3J(H,H) = 8 Hz, 4H), 7.12–76.90 (m, 18H), 062 (s, 6H).^{13}C NMR ($CDCl_3$, δ, ppm): 157.18, 155.30, 154.27, 140.97, 139.39, 136.84, 135.57, 133.75, 132.95, 131.81, 130.83, 130.77, 130.44, 128.79, 128.00, 127.21, 127.01, 126.73, 125.79, 125.53, 119.21, 118.94, −3.10. ^{29}Si NMR ($CDCl_3$, δ, ppm): 7.99. MS (FAB+, *m*-nitrobenzyl alcohol matrix) *m*/*z*: 951 $[M + H]^+$. Analysis calcd for $C_{70}H_{50}O_2Si$: 88.39 %C, 5.30 %H; found: 88.03 %C, 5.40 %H.

Silole C. Same procedure as for silole **B**, using a solution of 3,5-bis(2,2′-dipyridylamino)bromobenzene[37] **5** (1.43 g, 4.4 mmol) in THF (20 mL). After evaporation of the solvents, the resulting residue was subjected to silica gel column chromatography (MeOH–CH_2Cl_2 10 : 90) and recrystallized from a hexane–CH_2Cl_2 mixture to give **C** as a bright yellow powder (yield: 28%). Mp: 135–137 °C. UV-visible (λ_{max}, nm, logε): 282 (5.80), 303 (5.79), 379 (5.10). ^{1}H NMR ($CDCl_3$, δ, ppm): 8.31 (dd, ^3J(H,H) = 6, ^3J(H,H) = 2 Hz, 8H), 7.53 (td, ^3J(H,H) = 7, ^3J(H,H) = 2 Hz, 8H), 6.92–6.82 (m, 22H), 6.72–6.66 (m, 6H), 6.51 (d, ^3J(H,H) = 2 Hz, 4H), 0.27 (s, 6H).^{13}C NMR ($CDCl_3$, δ, ppm): 157.56, 154.46, 148.20, 145.25, 142.38, 141.19, 138.25, 137.76, 120.51, 127.41, 126.16, 123.49, 121.87, 118.33, 117.24, −4.11. ^{29}Si NMR ($CDCl_3$, δ, ppm): 8.67. MS (FAB+, *m*-nitrobenzyl alcohol matrix) *m*/*z*: 1091 $[M + H]^+$. Analysis calcd for $C_{70}H_{54}N_{12}Si$: 77.03 %C, 5.16 %H, 15.40 %N; found: 76.56 %C, 5.37 %H, 15.99 %N.

Silole D. Same procedure as for silole **B**, using a solution of **10** (2.76 g, 4.8 mmol) in THF (20 mL). The residue was purified by silica gel column chromatography (CH_2Cl_2–THF gradient 80 : 20 to 70 : 30) and crystallized from a hexane–CH_2Cl_2 mixture to afford **D** as a yellow solid (yield: 15%). Mp: 376 °C. UV-visible (λ_{max}, nm, logε): 268 (6.30), 389 (5.57), 407 (5.63). ^{1}H NMR ($CDCl_3$, δ, ppm): 8.45 (dd, ^3J(H,H) = 6, ^3J(H,H) = 2 Hz, 4H), 7.91–7.86 (m, 4H), 7.77–7.86 (m, 8H), 7.50–7.39 (m, 16H), 7.28–7.19 (m, 10H), 7.19–07.08 (m, 8H),

7.05–7.02 (m, 8H), 0.88 (s, 6H). ^{13}C NMR ($CDCl_3$, δ, ppm): 159.81, 159.33, 155.16, 148.90, 144.84, 141.53, 139.74, 139.29, 138.57, 137.56, 136.75, 136.29, 135.81, 133.48, 130.80, 130.42, 130.33, 129.50, 128.82, 127.85, 127.23, 127.03, 125.26, 125.14, 119.73, 118.37, 117.15, −4.54. ^{29}Si NMR ($CDCl_3$, δ, ppm): 8.27. MS (FAB+, *m*-nitrobenzyl alcohol matrix) *m*/*z*: 1257 $[M + H]^+$. Analysis calcd for $C_{90}H_{64}N_6Si$: 85.95 %C, 5.09 %H, 6.68 %N; found: 85.41 %C, 5.25 %H, 6.57 %N.

Silole E. A mixture of bis-silole **11** (0.40 g, 0.44 mmol), $Pd(PPh_3)_4$ (0.05 g, 0.044 mmol), and toluene (50 mL) was stirred for 10 min. The boronic acid **13**[40] (0.76 g, 26 mmol) in 20 mL of EtOH and NaOH (0.18 g) in 20 mL of H_2O were subsequently added. The mixture was stirred and refluxed for 72 h and allowed to cool to room temperature. The water layer was separated and extracted with CH_2Cl_2. The combined organic layers were dried over $MgSO_4$, and the solvents were evaporated under reduced pressure. Purification of the crude product was carried out by silica gel column chromatography (CH_2Cl_2–THF 85 : 15) followed by the recrystallization of the solid from a CH_2Cl_2–pentane mixture to afford **E** as a dark yellow solid in 86% yield. Mp: 334 °C. UV-visible (λ_{max}, nm, logε): 284 (5.77), 311 (5.79), 419 (5.65). ^{1}H NMR ($CDCl_3$, δ, ppm): 8.41 (dd, ^3J(H,H) = 6, ^3J(H,H) = 2 Hz, 4H), 7.66–7.57 (m, 8H), 7.39 (d, ^3J(H,H) = 8.5 Hz, 4H), 7.24 (d, ^3J(H,H) = 8.5 Hz, 4H), 7.07–6.96 (m, 24H), 6.88–6.83 (m, 4H), 6.72 (s, 4H), 0.53 (s, 12H). ^{13}C NMR ($CDCl_3$, δ, ppm): 157.62, 154.31, 153.68, 148.18, 141.58, 140.80, 139.04, 139.01, 138.96, 138.01, 137.14, 137.05, 129.98, 129.96, 129.37, 128.56, 128.13, 127.51, 127.41, 127.36, 126.36, 126.23, 126.15, 118.30, 116.95, −3.45. ^{29}Si NMR ($CDCl_3$, δ, ppm): 7.95. MS (FAB+, *m*-nitrobenzyl alcohol matrix) *m*/*z*: 1241 $[M + H]^+$. Analysis calcd for $C_{86}H_{68}N_6Si_2$: 83.18 %C, 5.51 %H, 6.78 %N; found: 82.87 %C, 5.67 %H, 6.80 %N.

X-Ray diffraction

The diffraction intensities for silole **11** were collected at the joint X-ray Scattering Service of the Institut Charles Gerhardt and the Institut Européen des Membranes of the University of Montpellier II, France, at 175 K using an Oxford Diffraction Xcalibur-I diffractometer. The structure was solved by *ab initio* (charge-flipping) methods using SUPERFLIP[54] and refined by least-squares methods on *F* using CRYSTALS,[55] against |*F*| on data having $I > 2\sigma(I)$; *R*-factors are based on these data. Hydrogen atoms were located from difference Fourier synthesis. The CH_2Cl_2 crystallization molecule was found to be heavily disordered. Two carbon positions and seven chlorine positions were found. The total site occupancy of the carbon positions was strongly restrained to 1 and that of the chlorine positions to 2. Restraints were also put on the U_{iso} parameters of carbon and chlorine in order to have them approximately equal. No attempts were made to place the proton sites for the two solvent carbon atoms. Basic structural data for silole **11** $C_{54}H_{44}Br_2Si_2{\cdot}2(CH_2Cl_2)$; two solvent hydrogens not placed: a = 13.8694(8) Å, b = 14.3213(8) Å, c = 26.3741(14) Å, α = 90°, β = 98.256(4)°, γ = 90°, V = 5184.4(5) Å^3, space group $C2_1/c$, 50 775 reflections measured, 3634 independent reflections with $I > 2\sigma(I)$ used for refinement with 307 parameters and two restraints. R = 0.0391. wR = 0.0383.

Device fabrication

Devices of *ca.* 10 mm^2 were fabricated on ITO-coated glass substrates (Merck, thickness ≈ 115 nm, sheet resistance $\rho \approx 17\ \Omega/\square$). After the cleaning process in trichloroethylene, ethanol and deionized water, a UV–ozone treatment was performed for 15 min. Then, a 50 nm thick layer of PEDOT-PSS was spin coated at 5000 rpm on top of ITO and baked at 80 °C for about 1 hour. PEDOT-PSS is a conducting polymer, acting as a buffer, in reducing short circuit problems induced by the ITO roughness. It weakly increases the work function of the anode and acts as a barrier to oxygen and indium diffusion from ITO.[56] On the PEDOT-PSS layer, the organic compounds as well as the cathodes were thermally evaporated under secondary vacuum (10^{-6} mbar). The deposition rate of the silole layer was set at about 1 nm s^{-1} with a thickness of 50 nm measured *in situ* using a quartz balance and *ex situ* using a Tencor AS-IQ profilometer. Finally, an 80 nm thick calcium layer capped by 100 nm thick aluminium layer was evaporated through a shadow mask on top of the silole derivative. Each preparation and characterization step took place in glove box under an inert atmosphere.

Acknowledgements

We thank the French ANR (PSICO project no. ANR-07-BLAN-0281-01) and the Région Languedoc-Roussillon for their financial support and for the award of a BDI thesis. We also thank Dr William Douglas for scientific discussions and technical assistance.

References

1 C. W. Tang and S. A. VanSlyke, *Appl. Phys. Lett.*, 1987, **51**, 913.
2 J. H. Burroughes, D. D. C. Bradley, A. R. Brown, R. N. Marks, K. Mackay, R. H. Friend, P. L. Burns and A. B. Holmes, *Nature*, 1990, **347**, 539.
3 D. F. O'Brien, M. A. Baldo, M. E. Thompson and S. R. Forrest, *Appl. Phys. Lett.*, 1999, **74**, 442.
4 M. A. Baldo, S. Lamansky, P. E. Burrows, M. E. Thompson and S. R. Forrest, *Appl. Phys. Lett.*, 1999, **75**, 4.
5 S. Lamansky, P. Djurovich, D. Murphy, F. Abdel-Razzaq, H. E. Lee, C. Adachi, P. E. Burrows, S. R. Forrest and M. E. Thompson, *J. Am. Chem. Soc.*, 2001, **123**, 4304.
6 S. Welter, K. Brunner, J. W. Hofstraat and L. De Cola, *Nature*, 2003, **421**, 54.
7 C. Borek, K. Hanson, P. I. Djurovich, M. E. Thompson, K. Aznavour, R. Bau, Y. Sun, S. R. Forrest, J. Brooks, L. Michalski and J. Brown, *Angew. Chem., Int. Ed.*, 2007, **46**, 1109.
8 M. Cocchi, J. Kalinowski, D. Virgili, V. Fattori, S. Develay and J. A. Williams, *J. Appl. Phys.*, 2007, **90**, 163508.
9 A. Fischer, S. Chénais, S. Forget, M.-C. Castex, D. Adès, A. Siove, C. Denis, P. Maisse and B. Geffroy, *J. Phys. D: Appl. Phys.*, 2006, **39**, 917.
10 G. Gu, G. Parthasarathy and S. R. Forrest, *Appl. Phys. Lett.*, 1999, **74**, 305.
11 M. Pfeiffer, K. Leo, X. Zhou, J. S. Huang, M. Hofmann, A. Werner and J. Blochwitz-Nimoth, *Org. Electron.*, 2003, **4**, 89.
12 J. Dubac, C. Guerin and P. Meunier, in *The Chemistry of Organic Silicon Compounds*, ed. Z. Rappoport and Y. Apeloig, Wiley, Chichester, 1998, vol. 2, pp. 1961–2036.
13 J. Dubac, A. Laporterie and G. Manuel, *Chem. Rev.*, 1990, **90**, 215.
14 S. Yamaguchi and K. Tamao, *J. Chem. Soc., Dalton Trans.*, 1998, 3693–3702.

15 J. Chen and Y. Cao, *Macromol. Rapid Commun.*, 2007, **28**, 1714.
16 S. Yamaguchi and K. Tamao, *Bull. Chem. Soc. Jpn.*, 1996, **69**, 2327.
17 N. Roques, P. Gerbier, U. Schatzschneider, J.-P. Sutter, P. Guionneau, J. Vidal-Gancedo, J. Veciana, E. Rentschler and C. Guérin, *Chem.–Eur. J.*, 2006, **12**, 5547.
18 N. Roques, P. Gerbier, J.-P. Sutter, P. Guionneau, D. Luneau and C. Guérin, *Organometallics*, 2003, **22**, 4833.
19 Cambridge Structural Database (CSD), 2003.
20 J. Chen, C. C. W. Law, J. W. Y. Lam, Y. Dong, S. M. F. Lo, I. D. Williams, D. Zhu and B. Z. Tang, *Chem. Mater.*, 2003, **15**, 1535–1546.
21 Y. Ren, Y. Dong, J. W. Y. Lam, B. Z. Tang and K. S. Wong, *Chem. Phys. Lett.*, 2005, **402**, 468.
22 H. Murata, Z. H. Kafafi and M. Uchida, *Appl. Phys. Lett.*, 2002, **80**, 189.
23 J. Chen, B. Xu, K. Yang, Y. Cao, H. H. Y. Sung, I. D. Williams and B. Z. Tang, *J. Phys. Chem. B*, 2005, **109**, 17086.
24 H. Y. Chen, W. Y. Lam, J. D. Luo, Y. L. Ho, B. Z. Tang, D. B. Zhu, M. Wong and H. S. Kwok, *Appl. Phys. Lett.*, 2002, **81**, 574.
25 L. Aubouy, P. Gerbier, N. Huby, G. Wantz, L. Vignau, L. Hirsch and J.-M. Janot, *New J. Chem.*, 2004, **28**, 1086.
26 H. Murata, G. G. Malliaras, M. Uchida, Y. Shen and Z. H. Kafafi, *Chem. Phys. Lett.*, 2001, **339**, 161–166.
27 N. Huby, G. Wantz, L. Hirsch, L. Vignau, A. S. Barrière, L. Aubouy and P. Gerbier, *J. Appl. Phys.*, 2006, **99**, 084907.
28 G. Yu, S. Yin, Y. Liu, J. Chen, X. Xu, X. Sun, D. Ma, X. Zhan, Q. Peng, Z. Shuai, B. Tang, D. Zhu, W. Fang and Y. Luo, *J. Am. Chem. Soc.*, 2005, **127**, 6335.
29 J. Pang, Y. Tao, S. Freiberg, X.-P. Yang, M. D'Iorio and S. Wang, *J. Mater. Chem.*, 2002, **12**, 206.
30 J. Lee, Q.-D. Liu, D.-R. Bai, Y. Kang, Y. Tao and S. Wang, *Organometallics*, 2004, **23**, 6205.
31 Z. H. Li, M. S. Wong, Y. Tao and H. Fukutani, *Org. Lett.*, 2007, **9**, 3659.
32 K. Danel, T. H. Huang, J. T. Lin, Y. T. Tao and C. H. Chuen, *Chem. Mater.*, 2002, **14**, 3860.
33 P. Raghunath, M. A. Reddy, C. Gouri, K. Bhanuprakash and V. J. Rao, *J. Phys. Chem. A*, 2006, **110**, 1152–1162.
34 S. Yamaguchi, T. Endo, M. Uchida, T. Izumizawa, K. Furukawa and K. Tamao, *Chem.–Eur. J.*, 2000, **6**, 1683–1692.
35 S. Murphy, X. Yang and G. B. Schuster, *J. Org. Chem.*, 1995, **60**, 2411.
36 F. Kong, X. L. Wu, G. S. Huang, R. K. Yuan, C. Z. Yang, P. K. Chu and G. G. Siu, *Appl. Phys. A: Mater. Sci. Process.*, 2006, **84**, 203–206.
37 W.-L. Jai, D.-R. Bai, T. McCormick, Q.-D. Liu, M. Motala, R.-Y. Wang, C. Seward, Y. Tao and S. Wang, *Chem.–Eur. J.*, 2004, **10**, 994.
38 M. Smet and W. Dehaen, *Molecules*, 2000, **5**, 620.
39 M. Smet, J. Van Dijk and W. Dehaen, *Tetrahedron*, 1999, **55**, 7859.
40 W.-L. Jia, D. Song and S. Wang, *J. Org. Chem.*, 2003, **68**, 701.
41 J. Lee, Q.-D. Liu, M. Motala, J. Dane, J. Gao, Y. Kang and S. Wang, *Chem. Mater.*, 2004, **116**, 1869–1877.
42 N. Huby, L. Hirsch, L. Aubouy, P. Gerbier and A. van der Lee, *Phys. Rev. B: Condens. Matter Mater. Phys.*, 2007, **75**, 115416.
43 C. Lee, W. Yang and R. G. Parr, *Phys. Rev. B: Condens. Matter Mater. Phys.*, 1988, **37**, 785.
44 M. J. Frisch, G. W. Trucks, H. B. Schlegel, G. E. Scuseria, M. A. Robb, J. R. Cheeseman, V. G. Zakrzewski, J. A. Montgomery, Jr., R. E. Stratmann, J. C. Burant, S. Dapprich, J. M. Millam, A. D. Daniels, K. N. Kudin, M. C. Strain, O. Farkas, J. Tomasi, V. Barone, M. Cossi, R. Cammi, B. Mennucci, C. Pomelli, C. Adamo, S. Clifford, J. Ochterski, G. A. Petersson, P. Y. Ayala, Q. Cui, K. Morokuma, D. K. Malick, A. D. Rabuck, K. Ragha-vachari, J. B. Foresman, J. Cioslowski, J. V. Ortiz, A. G. Baboul, B. B. Ste-fanov, G. Liu, A. Liashenko, P. Piskorz, I. Komaromi, R. Gomperts, R. L. Mar-tin, D. J. Fox, T. Keith, M. A. Al-Laham, C. Y. Peng, A. Nanayakkara, M. Challacombe, P. M. W. Gill, B. Johnson, W. Chen, M. W. Wong, J. L. Andres, C. Gonzalez, M. Head-Gordon, E. S. Replogle and J. A. Pople, *R. A. Gaussian 98*, Gaussian, Inc., Pittsburgh, PA, 1998.
45 L. Aubouy, N. Huby, L. Hirsch, A. Van der Lee and P. Gerbier, to be published.
46 H. Du, R. A. Fuh, J. Li, A. Corkan and J. S. Lindsey, *Photochem. Photobiol.*, 1998, **68**, 141.
47 S. Yamaguchi and K. Tamao, *Bull. Chem. Soc. Jpn.*, 1996, **69**, 2327.
48 C. Risko, G. P. Kushto, Z. H. Kafafi and J. L. Brédas, *J. Chem. Phys.*, 2004, **121**, 9031.
49 Y. Shirota and H. Kageyama, *Chem. Rev.*, 2007, **107**, 953.
50 K. Walzer, B. Maennig, M. Pefeiffer and K. Leo, *Chem. Rev.*, 2007, **107**, 1233.
51 L. Aubouy, P. Gerbier, C. Guérin, N. Huby, L. Hirsch and L. Vignau, *Synth. Met.*, 2007, **157**, 91.
52 V. Coropceanu, J. Cornil, D. A. da Silva Filho, Y. Olivier, R. Silbey and L.-L. Bredas, *Chem. Rev.*, 2007, **107**, 926.
53 F. Wang, J. Luo, J. Chen, F. Huang and Y. Cao, *Polymer*, 2005, **46**, 8422.
54 L. Palatinus and G. Chapuis, *J. Appl. Crystallogr.*, 2007, **40**, 786.
55 P. W. Betteridge, J. R. Carruthers, R. I. Cooper, K. Prout and D. J. Watkin, *J. Appl. Crystallogr.*, 2003, **36**, 1487.
56 A. V. Dijken, A. Perro, E. A. Meulenkamp and K. Brunner, *Org. Electron.*, 2003, **4**, 131–141.

